Materials Science & Engineering A 571 (2013) 199–206

Contents lists available at SciVerse ScienceDirect

Materials Science & Engineering A

journal homepage: www.elsevier.com/locate/msea

Effects of extrusion deformation on microstructure, mechanical properties and hot workability of β containing TiAl alloy

W.C. Xu [a,*], D.B. Shan [a], H. Zhang [b], X.A. Li [a], Y.Z. Zhang [c], S. Nutt [c]

[a] School of Materials Science and Engineering, Harbin Institute of Technology, Harbin 150001, PR China
[b] Aerospace Research Institute of Materials & Processing Technology, Beijing 100076, PR China
[c] Department of Chemical Engineering and Materials Science, University of Southern California, Los Angeles, CA 90089-0241, USA

ARTICLE INFO

Article history:
Received 7 November 2012
Received in revised form
30 January 2013
Accepted 1 February 2013
Available online 9 February 2013

Keywords:
Intermetallics
TiAl alloys
Hot extrusion
Mechanical properties
Hot workability

ABSTRACT

Hot extrusion was performed on a Ti–42Al–9V–0.3Y alloy at 1200–1325 °C to explore effects on mechanical properties and hot workability. The microstructure after hot extrusion was analyzed, tensile tests were conducted, and hot workability was assessed. Three types of microstructures resulted from extrusion at increasing temperature, including a dual-phase microstructure (DPM), a bi-lamellar microstructure with retained gamma phase (BLMG), and a bi-lamellar microstructure (BLM). Hot extrusion of the TiAl alloy in the range of 1275–1325 °C produced the BLM microstructure, yielding superior comprehensive properties. The predominant fracture mode was transgranular cleavage fracture in the DPM, translamellar cleavage and delamination in BLM, and mixed fracture in BLMG. Aggregation of the YAl_2 phase accelerated the fracture of the as-extruded alloy. As-extruded Ti–42Al–9V–0.3Y alloy exhibited excellent high-temperature mechanical properties and hot workability, demonstrating the feasibility of precision forming TiAl alloy components by conventional hot forging with nickel-based alloy dies.

1. Introduction

Alloys based on γ-TiAl are promising materials for high-temperature structural applications in aerospace and automobile engine components, including blades, vanes or discs, and turbochargers because of exceptional high-temperature strength, low density, and good oxidation resistance [1–4]. However, low ductility, poor fracture toughness and limited hot workability arise from the intrinsic brittleness of γ and α_2 ordered phases and limit the use of such alloys [5]. In addition, coarse-grained microstructures, casting texture, and chemical inhomogeneity typically characterize γ-TiAl cast ingots [6–8]. For high-risk applications, these microstructural deficiencies are a serious concern. Recent reports indicate that hot working can reduce casting inhomogeneity, refine as-cast coarse grains, and greatly improve the mechanical properties of the products [9–15]. Unfortunately, γ-TiAl alloys have limited hot workability, thus limiting the utility of hot deformation in practical production.

An effective way to improve the hot deformability of TiAl alloys is through introduction of β phase [16–20]. Tetsui et al. developed new TiAl alloys (Ti–42Al–5Mn [21] and Ti–42Al–10 V (at%) [22]) containing β phase inclusions, and showed that these could be hot formed above 1250 °C by free forging or closed-die forging. Similarly, Li et al. introduced Y to refine the microstructure of Ti–43Al–9V, resulting in improved ductility in the as-cast β-containing γ-TiAl alloys, albeit with reduced strength [23].

Hot extrusion is often used to breakdown coarse microstructures of as-cast ingots of TiAl alloys and for fabrication of high-performance rods and preforms [24,25]. However, there have been no systematic studies describing how to improve the mechanical properties and hot workability of β-containing TiAl alloys by hot extrusion. In the present study, the effects of hot extrusion on microstructural evolution and mechanical properties of a Ti–42Al–9V–0.3Y β-containing alloy are investigated. Hot extrusion was conducted at 1200–1325 °C. Microstructural analysis and tensile tests were carried out before and after hot extrusion, and hot workability was analyzed using hot processing window maps validated through isothermal forging experiments.

2. Experimental

An ingot with the nominal composition Ti–42Al–9V–0.3Y (at%) was prepared by induction skull melting (ISM) and casting into a steel mold to produce a sample Φ120 × 200 mm. Before hot extrusion, the ingot was hot isostatic pressed (HIP) at 1250 °C/175 MPa for 4 h to eliminate casting porosity. The composition, determined by X-ray fluorescence spectroscopy, was 41.49% Al,

* Corresponding author. Tel.: +86 451 86416221; fax: +86 451 86418640.
E-mail address: xuwc_76@hit.edu.cn (W.C. Xu).

0921-5093/$ - see front matter © 2013 Elsevier B.V. All rights reserved.
http://dx.doi.org/10.1016/j.msea.2013.02.005

9.4% V, 0.26% Y and the balance Ti. The phase transformation temperatures were measured by differential scanning calorimetry (DSC) following the proposed ternary phase diagram for Ti–Al–V [26], revealing that $T_{\beta+\gamma+\alpha_2\rightarrow\beta+\gamma+\alpha}$ was ~1209 °C, $T_{\beta+\gamma+\alpha\rightarrow\beta+\alpha}$ was ~1267 °C, and $T_{\beta+\alpha\rightarrow\beta}$ was ~1333 °C.

Cylindrical billets 42 mm in diameter × 35 mm in length were cut from the ingot by electrical discharge machining (EDM), and the billets were insulated by ceramic fiber blankets and capsulated in 5 mm thick stainless steel cans. After heating to the selected extrusion temperatures and holding for 60 min, the samples were extruded in a single pass using a hydraulic press of 3150 kN and the reduction in area was 1/9. Six extrusion temperatures were selected in the range of 1200–1325 °C in different phase regimes to study microstructure evolution and mechanical properties of the TiAl alloy.

The mechanical properties were measured by tensile experiments using a load frame (Instron-5500R), and hot workability was evaluated by compression experiments on a simulator (Gleeble-1500). Tensile specimens with gauge section Φ3 × 21 mm and cylindrical compressed specimens of Φ8 × 12 mm were cut from the extruded billet with the loading direction parallel to the extrusion direction. Tensile tests were conducted at room temperature (RT) and 700 °C at a strain rate of $3.75\times10^{-4}\,s^{-1}$, and compression experiments were performed at strain rates from 10^{-3} to $1\,s^{-1}$ at 950–1150 °C.

Microstructures were observed by scanning electron microscopy (SEM) and transmission electron microscopy (TEM). Samples for SEM observation were etched in a Kroll's reagent of 5% HNO_3, 3% HF and 92% H_2O (vol%). Samples for TEM observation were prepared by twin-jet polishing using a solution of 60% methanol, 35% butyl alcohol and 5% perchloric acid at −3 °C and 35 V. Fracture surfaces of tensile specimens were observed by SEM.

3. Results and discussion

3.1. Microstructure evolution during hot extrusion

Fig. 1 presents the XRD pattern of the as-cast Ti–42Al–9V–0.3Y alloy, and the pattern indicated that the TiAl alloy was composed primarily of γ and β phase. Fig. 2 shows the cast microstructure, which exhibited γ phase (dark contrast) distributed evenly in the β matrix (graywhite contrast). Energy dispersive X-ray spectroscopy (EDS) indicated that the β phase contained a high V content (22.31 at%) while the γ phase was rich in Al. There was much more β phase relative to other TiAl alloys due to the introduction of β-stabilizing V element. In addition, particles were distributed in a discontinuous network along as-cast grain boundaries (bright

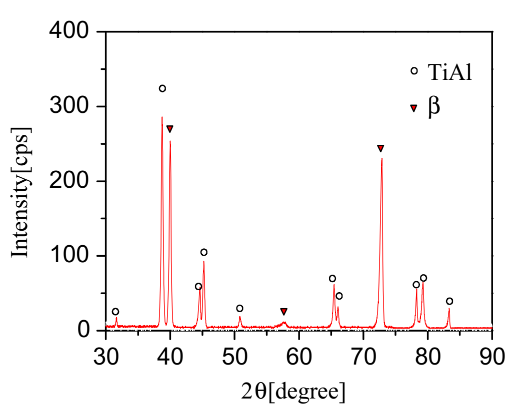

Fig. 1. XRD pattern of Ti–42Al–9V–0.3Y.

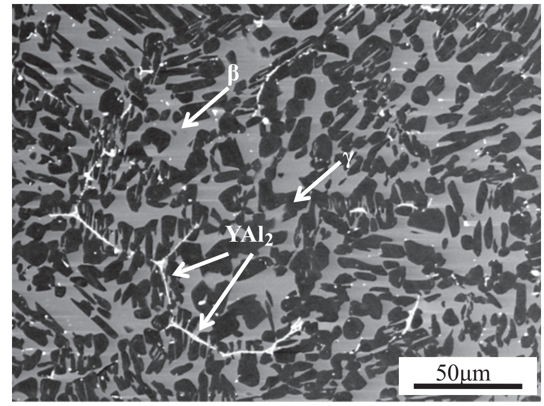

Fig. 2. BSE micrograph of the as-cast Ti–42Al–9V–0.3Y alloy.

contrast), identified as YAl_2, which was below the detectability limit of the XRD analysis.

The microstructures after hot extrusion at 1200–1325 °C are shown in Fig. 3. Extrusion temperatures of 1200 °C–1225 °C and 1275–1325 °C are in the $\beta+\gamma+\alpha_2$, $\alpha+\beta+\gamma$ and $\alpha+\beta$ phase fields, respectively. When specimens were extruded at 1200 °C, massive γ phase appeared as elongated inclusions (Fig. 3b). Also, β phase supersaturated with Al precipitated as strips of γ phase during air cooling. At an extrusion temperature of 1225 °C, the amounts of both retained massive γ and β phases decreased markedly, and lamellar colonies of α/γ and β/γ appeared (Fig. 3c and d). As the extrusion temperature was increased to 1275 °C and beyond, the retained massive γ phase disappeared almost completely (Fig. 3e–h). At these temperatures, the α_2/γ lamellae grew gradually and uniformly, comprising increasing volume fractions of the matrix (Fig. 3e–j). Detailed microstructure descriptions are listed in Table 1. The as-extruded microstructures are categorized into dual phase microstructure (DPM), bi-lamellar microstructure with retained gamma phase (BLMG), and bi-lamellar microstructure (BLM), respectively, according to the microstructural evolution at 1200–1325 °C.

TEM images of the microstructures after hot extrusion are presented in Fig. 4. Fig. 4a shows dislocated γ twins, while Fig. 4b and c shows recrystallized grains of retained massive γ and β subgrains, respectively. Fig. 4d and e shows α_2/γ and β/γ lamellar structures, determined by diffraction analysis. Fig. 4f shows retained β phase between α_2/γ lamellar colonies. Because of the high extrusion speeds and limited slip systems available, twinning occurred during hot extrusion, typically in the retained massive γ grains (Fig. 4a). The large extrusion strains and high temperatures induced localized dynamic recrystallization of the γ grains (Fig. 4b and g). In contrast, the dislocation density was typically much lower in β grains, and many β subgrains appeared due to dynamic recovery (Fig. 4c and h). Streaks in diffraction patterns from the β phase presumably resulted from elastic distortion of the crystal lattice originating from compositional fluctuation in the $\beta\rightarrow B_2$ ordering transformation during air cooling [27]. Typically, β grains were distributed along the boundaries of lamellar α_2/γ colonies (Fig. 4f). Because the disordered β phase with bcc lattice provides enough independent slip systems at high temperature, β phases are more easily deformed and dynamically softened [16,28], which could work like a lubricating layer to coordinate plastic deformation of harder α_2/γ phases [29], thus contributing to the enhanced hot deformability of the Ti42Al9V0.3Y alloy.

Microstructures extruded at 1275 °C were characterized by lamellar α_2/γ and β/γ structures, as shown in Fig. 4 d–e. Because large quantities of V-rich β phase remain in the as-cast microstructure, they were not completely dissolved in the

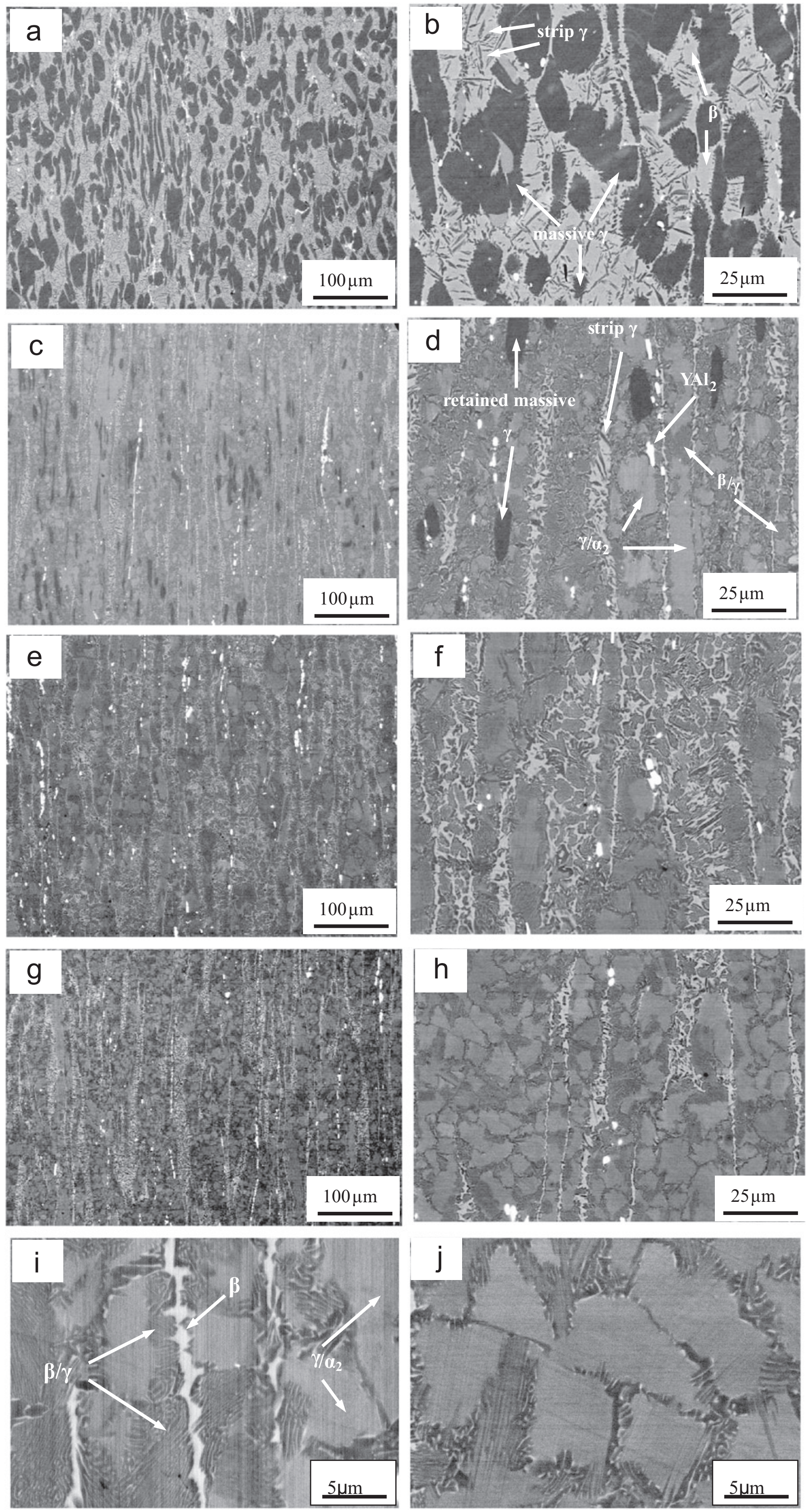

Fig. 3. Microstructures of Ti–42Al–9V–0.3Y alloy extruded at: (a and b) 1200 °C; (c and d) 1225 °C; (e and f) 1275 °C; (g and h) 1325 °C. Images (i) and (j) show enlargements of (e and f) 1275 °C and (g and h) 1325 °C.

matrix because the limited preheating time and high extrusion speeds did not allow for complete diffusion. In the subsequent air-cooling process, the phase transition of the as-extruded microstructure proceeds as follows: $\beta \rightarrow \beta + \alpha \rightarrow$ lamellar(α/γ)+ $\beta \rightarrow$ lamellar(α_2/γ)+β+γ, in accordance with the Ti–Al–V ternary phase diagram [26]. The phase transformation of hexagonal

Table 1
Microstructures after hot extrusion at different temperatures.

Temperature (°C)	1200	1225	1275	1325
Microstructure	Massive γ phase	Massive γ phase	–	–
	Strip γ phase	Strip γ phase	Strip γ phase	Strip γ phase
	Retained β phase	Retained β phase	Retained β phase	Retained β phase
	YAl_2	YAl_2	YAl_2	YAl_2
	–	α_2/γ Lamellae	α_2/γ Lamellae	α_2/γ Lamellae
	–	β/γ Lamellae	β/γ Lamellae	β/γ Lamellae
Name	DPM	BLMG	BLM	BLM

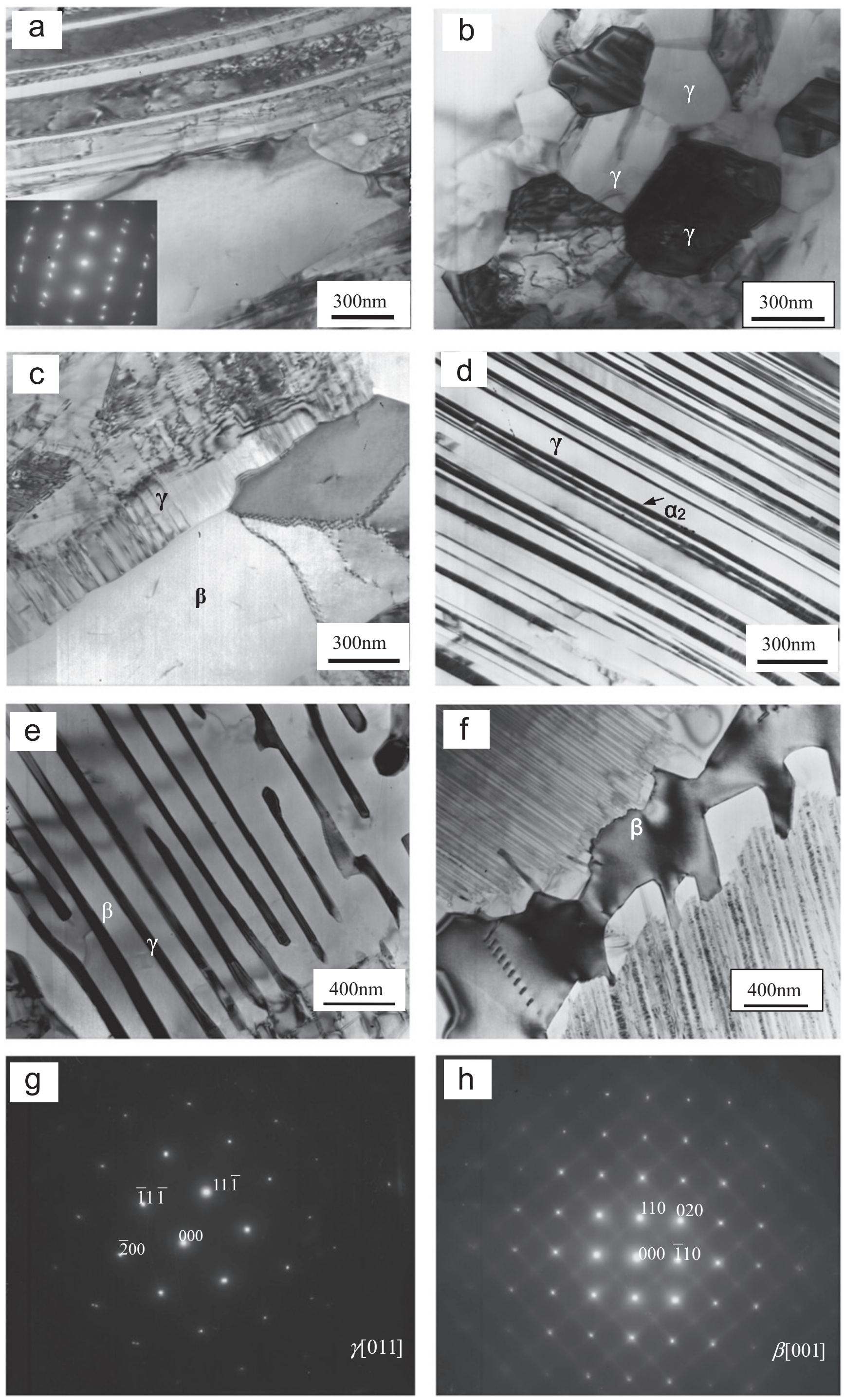

Fig. 4. TEM images of hot-extruded microstructures showing: (a) dislocated twinned γ grains after extrusion at 1225 °C; (b) recrystallized grains of retained massive γ and (c) subgrains of retained massive β after extrusion at 1225 °C; Lamellae of (d) α_2/γ after extrusion at 1275 °C and of (e) β/γ after extrusion at 1325 °C; (f) β grains on boundaries of lamellar colonies after extrusion at 1325 °C; (g) diffraction pattern of γ phase in Fig. 3b and (h) diffraction pattern of β phase in (c).

close-packed (hcp) $\alpha \rightarrow$face-centered cubic (fcc) γ reportedly proceeds by propagation of Shockley dislocations [30], leading to the formation of a two-phase α/γ lamellar structure with the orientation relationship $(111)_\gamma//(0001)_\alpha$ and $(1\overline{1}0)_\gamma//(11\overline{2}0)_\alpha$ in elongated α grains (Fig. 3d). The γ-phase strips precipitated in elongated β grains (Fig. 2d), and the β/γ lamellae occurred adjacent to α_2/γ colonies (Fig. 3i–j), although no definite orientation relationship was observed between β and γ phases. The dissolution of the retained V-rich β phase accelerated with increasing extrusion temperature, reducing the quantity of retained β in high-temperature extrusions (Fig. 3h).

3.2. Mechanical properties and fracture analysis of as-extruded microstructure

Fig. 5 shows the tensile strength and elongation at room temperature (RT) as a function of extrusion temperature. With increasing extrusion temperature, the yield strength (YS) and ultimate tensile strength (UTS) first increased 30–50%, then decreased, and conversely the elongation percentage (δ) first decreased ~30%, then increased. When the extrusion temperature exceeded 1275 °C, the strength and ductility were relatively stable and showed little temperature dependence. The maximum and minimum δ (1.67% and 1.22%) occurred at extrusion temperatures of 1200 °C and 1225 °C, respectively, and the maximum and minimum UTS (1217 MPa and 937.8 MPa) occurred at extrusion temperatures of 1225 °C and 1200 °C.

When the material was extruded at 1200 °C, the microstructure exhibited minimum strength and maximum ductility because of the prevalence of the relatively soft β/B2 phases. In contrast, at extrusion temperatures >1225 °C (in the $\alpha+\beta+\gamma$ phase regime), lamellar structures (α_2/γ and β/γ) characterized the as-extruded microstructures (Fig. 3c–h). Interfaces between α_2/γ and β/γ inhibited dislocation slip during deformation [31] and promoted alloy strength. Increasing the extruding temperature caused gradually increases in the average size, lamellar spacing and volume fraction of the α_2/γ colonies. The average α_2/γ lamellar colony size and lamellar spacing were ~8 μm and ~40 nm, respectively, after extrusion at 1225 °C, and the colony dimensions grew to >12 μm and 60 nm after extrusion at ≥1275 °C. Microstructural refinement resulted in the greatest strength after extrusion at 1225 °C. However, alloy samples extruded at this temperature showed the least elongation, which was attributed to multi-phase mixed microstructural nonuniformity (TLMG in Table 1) [32]. In addition, the finest spacing of α_2/γ and β/γ formed after extrusion at 1225 °C and suppressed hard

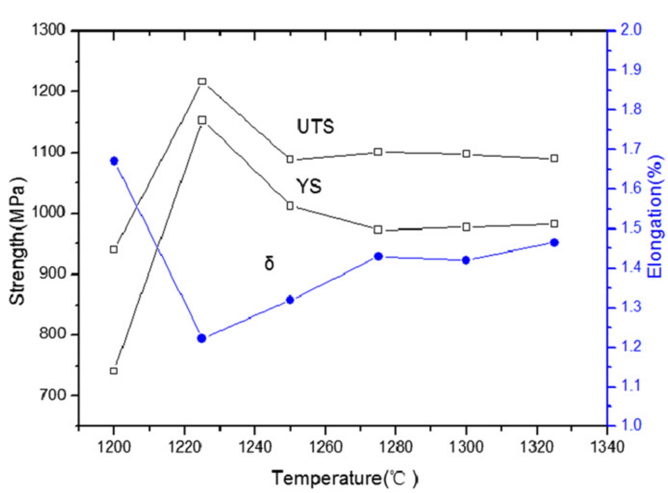

Fig. 5. Tensile properties of Ti–42Al–9V alloy extruded at different temperatures.

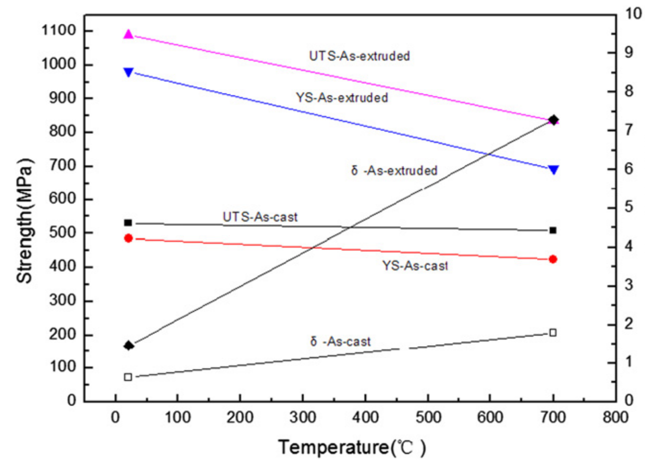

Fig. 6. Tensile properties of as-cast and as-extruded Ti–42Al–9V alloy at different temperatures.

deformation modes, particularly cross twins, which contributed to the reduced ductility of the as-extruded alloy [33].

Fig. 6 shows the temperature dependence of the tensile properties for as-cast and as-extruded conditions. The strength and elongation of the hot-extruded Ti–42Al–9V–0.3Y alloy were significantly greater than those of the as-cast material, regardless of test temperature. The room temperature tests on the extruded alloy showed increases in UTS (from 530 MPa to 1090 MPa) and elongation (from 0.63% to 1.47%) compared to the as-cast alloy. Similarly, tests conducted at 700 °C showed increases in UTS (from 509 MPa to 837 MPa) and elongation (from 1.8% to 7.3%) compared to the as-cast microstructure.

Fractographs of tensile samples fractured at different temperatures are shown in Fig. 7. The fracture mode of the alloy extruded at 1200 °C was predominantly transgranular cleavage with numerous cleavage planes of γ and β phases (the main cleavage planes in γ are {111}) [10,32]. The fracture transformed to a mixed mode of transgranular, translamellar and delamination fracture because extrusion at 1225 °C produced retained massive γ phase (leading to transgranular cleavage fracture) and lamellar colonies of α_2/γ and β/γ phases (leading to translamellar and delamination fracture). In material extruded ≥1275 °C, the fracture was dominated by transgranular failure, including translamellar cleavage and delamination (Fig. 7b–d). In the β/γ lamellar structure, the β phase was discontinuous and irregular, and no definite orientation relationship existed between β and γ phase. Thus, cracks propagated along translamellar pathways in the β/γ microstructure. In α_2/γ lamellar colonies, both delamination along α_2/γ interfaces (Fig. 7c) and translamellar fracture occurred during room temperature fracture. In addition, YAl_2 particles were evident on the fracture surface (Fig. 7d), a result of detachment between YAl_2 and matrix phases. Aggregation of YAl_2 accelerated the fracture of as-extruded microstructure (Fig. 3d and Fig. 7d).

Observations of fracture surfaces of as-extruded and as-cast specimens tested at 700 °C (Fig. 7e and f) indicated that the fracture was primarily translamellar and delamination in the extruded alloy, while the fracture mode was primarily intergranular and brittle in the as-cast alloy. Grain refinement increases both the strength and ductility of the as-extruded alloy according to Hall–Petch relationship. In addition, the lamellar character of the as-extruded microstructures results in microcrack shielding, thereby increasing the ductility and strength of the as-extruded alloy [5,34]. These observations indicate that the hot extrusion process can be optimized for the TiAl alloy in the 1275–1325 °C window to produce various lamellar microstructures by design,

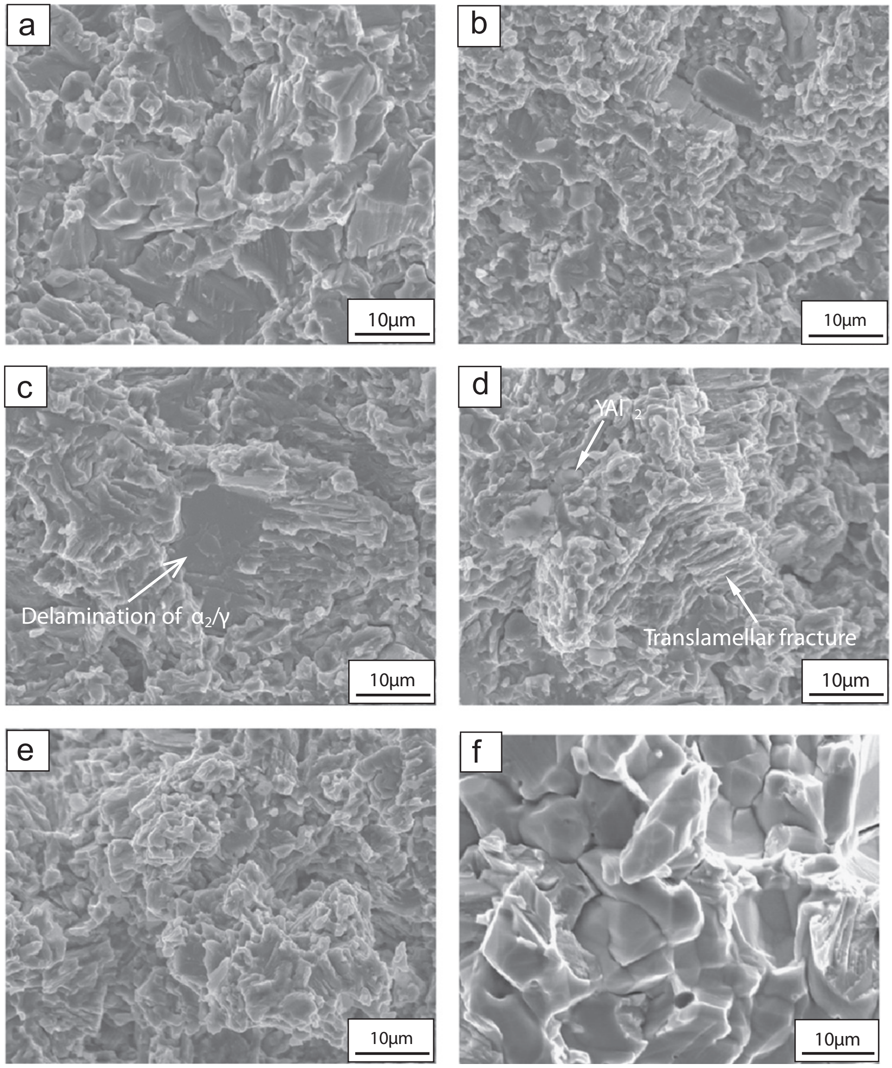

Fig. 7. Tensile fracture surfaces of samples hot extruded Ti42Al9V0.3Y alloy tested at room-temperature: (a) after extrusion at 1200 °C; (b) after extrusion at 1225 °C; (c) after extrusion at 1250 °C and (d) after extrusion at 1300 °C, tensile fracture surfaces after testing at 700 °C for (e) as-extruded and (f) as-cast at 1325 °C.

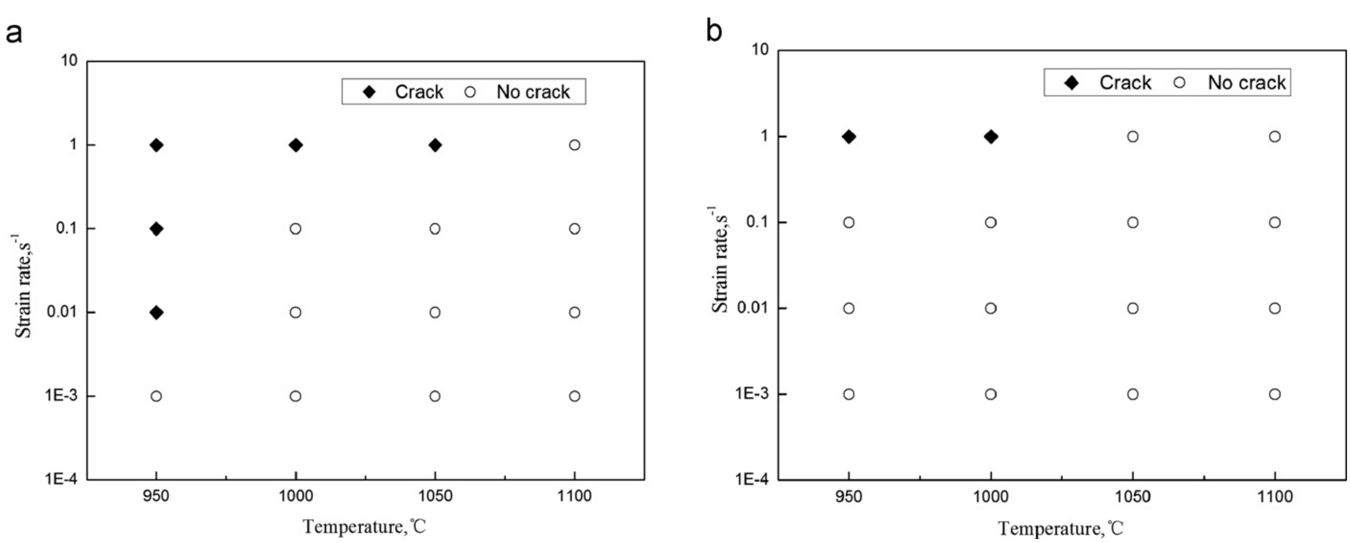

Fig. 8. Deformation window of Ti–42Al–9V alloy. (a) as-cast and (b) as-extruded.

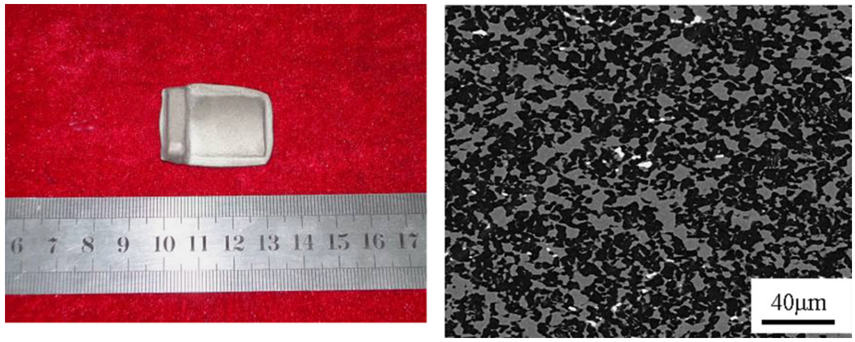

Fig. 9. Photograph and microstructure of TiAl compressor blade by conventional isothermal forging.

i.e., by judiciously selection of microstructures to achieve specific combinations of mechanical properties.

3.3. *Hot workability of as-extruded microstructure*

Fig. 8 shows the deformation windows for the as-cast and as-extruded alloys in hot compression experiments with 50% engineering compressive strain. For the as-cast alloy compressed at 950 °C, cracks occurred at higher strain rates ($\geq 0.01\ s^{-1}$). When the deformation temperature was increased above 1000°, cracks were observed only at 1000–1050 °C and $\dot{\varepsilon} = 1\ s^{-1}$ (Fig. 8a), demonstrating the excellent hot workability of the alloy. After hot extrusion, cracks appeared only at 950–1000 °C and $\dot{\varepsilon} = 1\ s^{-1}$ (Fig. 8b), indicating a further increase in the hot workability of the alloy. The enhanced hot workability of the alloy is attributed to the introduction of β phase (via V addition) and microstructural refinement (from Y addition and extrusion deformation). Because of the improved workability of the alloy, parts can be deformed at 950 °C and even below, and it is possible to hot forge alloy parts using traditional nickel-based alloy dies. Fig. 9 shows a small blade of Ti–42Al–9V–0.3Y alloy produced by isothermal die forging at 1050 °C × 0.5 s^{-1} in an argon atmosphere (the blade billets were not encapsulated during isothermal die forging). The refined microstructure is uniform with minimal aggregation. Thus, an optimized hot-extrusion process can yield TiAl alloy parts with improved hot working characteristics, and the hot-forged parts show uniform microstructure and improved mechanical properties. Furthermore, the ability to use conventional forging methods for β containing TiAl alloy is likely to reduce production costs significantly.

4. Conclusions

The effects of extrusion on microstructural evolution, mechanical properties and hot workability of a β-containing TiAl alloy (Ti–42Al–9V–0.3Y) were investigated. The main conclusions are summarized below.

(1) Three types of microstructures were obtained from hot-extrusion, including dual-phase microstructure (DPM), bi-lamellar microstructure with retained gamma phase (BLMG), and bi-lamellar microstructure (BLM). The DPM was primarily composed of massive γ phase and β phase, the BLMG primarily consisted of α_2/γ and β/γ lamellae with retained massive γ and β phase, and the BLM primarily consisted of α_2/γ and β/γ lamellae with retained β. The α/γ lamellar structure exhibited the orientation relationship of $(111)_\gamma//(0001)_\alpha$ and $(1\overline{1}0)_\gamma//(11\overline{2}0)_\alpha$ while the β/γ lamellae showed no consistent orientation relationship.

(2) With increasing extrusion temperature, YS and UTS first increased then decreased, and δ first decreased then increased. The DPM showed the greatest room-temperature ductility and lowest strength, observations that were attributed to the presence of soft β/B2 phases. The BLMG showed opposite trends compared with DPM due to the refined microstructure with non-uniform distribution of retained massive γ. Optimal microstructure/properties for the TiAl alloy were achieved by extrusion at 1275–1325 °C, and the BLM microstructure resulted in superior comprehensive properties.

(3) The dominant fracture mode was transgranular cleavage fracture in the DPM, translamellar cleavage and delamination in BLM, mixed fracture in the BLMG. Aggregation of YAl_2 accelerated the fracture of as-extruded microstructures.

(4) Hot-extrusion of the TiAl alloy increased both strength and ductility relative to as-cast properties. The high-temperature mechanical properties and hot workability were also increased by hot-extrusion. The β-containing TiAl alloy can be hot-formed at relatively low cost by conventional forging methods using traditional nickel-based alloy dies.

Acknowledgments

The work was supported by 1st Special National Postdoctor Foundation of China and Youth Science and Technology Project of Harbin City (Grant no. 2008RFQXG040). Authors also acknowledge support from the China Scholarship Council and the M.C. Gill Composites Center at the University of Southern California.

Appendix A. Supporting information

Supplementary data associated with this article can be found in the online version at http://dx.doi.org/10.1016/j.msea.2013.02.005.

References

[1] Y.W. Kim, D.M. Dimiduk, J. Met. 46 (1994) 30–39.
[2] G. Das, H. Kestler, H. Clemens, P.A. Bartolotta, J. Met. 56 (2004) 42–45.
[3] M. Yamaguchi, H. Inui, K Ito, Acta Mater. 48 (2000) 307–322.
[4] X. Wu, D. Hu, M.H. Loretto, J. Mater. Sci. 39 (2004) 3935–3940.
[5] R. Gao, L. Li, J.H. Chen, J. Zhang, Mater. Sci. Eng. A 527 (2010) 2468–2477.
[6] F. Appel, R. Wagner, Mater. Sci. Eng. R 22 (1998) 187–268.
[7] Z.W. Huang, Scr. Mater. 52 (2005) 1021–1025.
[8] V. Imayev, T. Khismatullin, T. Oleneva, R. Imayev, R. Valiev, R. Wunderlich, A. Minkow, U. Hecht, H.J. Fecht, Adv. Eng. Mater. 10 (2008) 1095–1100.
[9] M. Oehring, U. Lorenz, J. Paul, F. Appel, Mater.Sci. Forum 426–432 (2003) 1685–1690.
[10] M. Hasegawa, H. Fukutomi, Mater. Sci. Eng. A 508 (2009) 106–113.
[11] S.L. Semiatin, V. Seetharaman, V.K. Jain, Metall. Trans. A 25 (1994) 2753–2768.

[12] W.J. Zhang, U. Lorenz, F. Appel, Acta Mater. 48 (2000) 2803–2813.
[13] X.J. Xu, J.P. Lin, Y.L. Wang, J.F. Gao, Z. Lin, G.L. Chen, J. Alloys Compd. 414 (2006) 175–180.
[14] L. Wang, Y. Liu, W. Zhang, H. Wang, Q. Li, Intermetallics 19 (2011) 68–74.
[15] T. Tetsui, K. Shindo, S. Kobayashi, M. Takeyama, Intermetallics 11 (2003) 299–306.
[16] J.D. Shi, Z.J. Pu, Z.Y. Zhong, D.X. Zou, Scr. Metall. Mater. 27 (1992) 1331–1336.
[17] D. Vanderschueren, M. Nobuki, M. Nakamura, Scr. Metall. Mater. 28 (1993) 605–610.
[18] T. Tetsui, T. Kobayshi, H. Harada, Mater. Sci. Eng. A 552 (2012) 345–352.
[19] H. Clemens, W. Wallgram, S. Kremmer, V. Güther, A. Bartels, Adv. Eng. Mater. 10 (2008) 707–713.
[20] H. Clemens, H.F. Chladil, W. Wallgram, G.A. Zickler, R. Gerling, K.D. Liss, S. Kremmer, V. Guther, W. Smarsly, Intermetallics 16 (2008) 827–833.
[21] T. Tetsui, K. Shindo, S. Kaji, S. Kobayashi, M. Takeyama, Intermetallics 13 (2005) 971–978.
[22] T. Tetsui, K. Shindo, S. Kobayashi, M. Takeyama, Scr. Mater. 47 (2002) 399–403.
[23] B.H. Li, Y.Y. Chen, Z.Q. Hou, F.T. Kong, J. Alloys Compd. 473 (2009) 123–126.
[24] J.Y. Si, F. Gao, P.B. Han, J. Zhang, Intermetallics 19 (2011) 169–174.
[25] C.G. Bai, D. Liu, D.S. Xu, Y.Y. Cui, Y.L. Hao, R. Yang, Mater. Sci. Forum 475-479 (2005) 789–794.
[26] M. Takeyama, S. Kobayashi, Intermetallics 13 (2005) 993–999.
[27] M. Premkumar, K.S. Prasad, A.K. Singh, Intermetallics 17 (2009) 142–145.
[28] J.S. Kim, Y.H. Lee, Y.W. Kim, C.S. Lee, Mater. Sci. Forum 539–543 (2007) 1531–1536.
[29] J.G. Wang, T.G. Nieh, Intermetallics 8 (2000) 737–748.
[30] A. Denquin, S. Naka, Acta Metall. Mater. 44 (1996) 343–352.
[31] D. Hu, M.H. Loretto, Intermetallics 7 (1999) 1299–1306.
[32] K. Maruyama, N. Yamada, H. Sato, Mater. Sci. Eng. A 319–321 (2001) 360–363.
[33] J. Zhang, J.D. Shi, D.X. Zou, Z.Y. Zhong, Scr. Mater. 34 (1996) 1815–1818.
[34] Y.W. Kim, Intermetallics 6 (1998) 623–628.